symmetry

Article

On-Chip Design of a Broadband 850 nm TM-Pass/TE-Stop Polarizer with Tilted Subwavelength Gratings

Yue Dong *, **Yu Liu, Yin Xu and Bo Zhang**

Department of Electric Engineering, School of Internet of Things Engineering, Jiangnan University, No. 1800 Lihu Avenue, Wuxi 214122, China
* Correspondence: y.dong@jiangnan.edu.cn

Abstract: An integrated TM-pass/TE-stop polarizer centered at 850 nm is designed in this paper. The proposed polarizer is designed on a Si_3N_4 on insulator platform with tilted subwavelength gratings (SWG). Since the tilted SWGs have much more of an impact on the effective index of the TE polarization state than that of the TM polarization state, they help to achieve high TM and low TE transmission simultaneously. After geometries optimization, the polarizer's working bandwidth, which is defined as the wavelength region with an extinction ratio higher than 20 dB, is determined to be 185 nm under a SWG tilting angle of 30 degrees. At the same time, the insertion loss is always less than 0.45 dB over the entire working wavelength band. Finally, the results of fabrication tolerance analysis show that the SWG ridge width jitter only degrades the polarizer's working bandwidth by 16 nm.

Keywords: polarizer; TM-pass/TE-stop; tilted subwavelength gratings

check for updates

Citation: Dong, Y.; Liu, Y.; Xu, Y.; Zhang, B. On-Chip Design of a Broadband 850 nm TM-Pass/TE-Stop Polarizer with Tilted Subwavelength Gratings. *Symmetry* **2022**, *14*, 2359. https://doi.org/10.3390/sym14112359

Academic Editor: Christophe Humbert

Received: 18 October 2022
Accepted: 7 November 2022
Published: 9 November 2022

1. Introduction

Polarization management [1] is one of the most critical issues in photonic integrated circuits (PICs). To date, a number of passive integrated devices, including the polarization beam splitter (PBS) [2–4], the polarization splitter and rotator (PSR) [5–7], and the polarizer [8,9], have been proposed to realize various different kinds of polarization control functions. The PBS and PSR normally use a symmetrical or asymmetrical directional coupler to divide the incident lightwave into two separated waveguides. Hence, it has to meet the critical phase matching conditions. In contrast, the polarizer is an easier polarization manipulating solution that allows only one of the polarization states to pass.

Many device principles have been reported for polarizer design and implementation. As an example, hybrid plasmonic gratings (HPG) [10,11] were utilized to realize compact and broadband polarizers with a footprint of only a few micrometers. However, the absorption of the HPG waveguide normally results in an unacceptably high insertion loss. Another example for polarizer realization is the Bragg grating [12,13]. With the assistance of chirped gratings, such a Bragg grating-based polarizer achieves an ultra-broad bandwidth greater than 200 nm. Unfortunately, the strong reflection of Bragg gratings may damage the prepositioned devices such as insulator [14] and circulator [15]. Subwavelength grating (SWG) [16] is another widely used polarizer structure which normally works in leakage mode principles [17]. By setting the appropriate SWG geometries, the unwanted polarization state will be leaked into the claddings.

Up to now, most polarizers have been designed for 1550 nm, which is widely used in communication applications. However, in life science [18] applications, 1550 nm normally has strong absorption in biomedical tissues. Additionally, the microscopic [18] and tomographic [19] technologies for fine structure inspection require microscale or even sub-microscale spatial resolution that is unresolvable at 1550 nm. In this case, the integrated photonic technologies have to extend the working wavelength region shorter than

1 μm [18–20], e.g., 850 nm or even the visible wavelength region. In addition, TE-pass polarizers are much more discussed in all above-mentioned works than TM-pass polarizers. In practice, the TM polarization state has stronger interactions of evanescent waves that are more useful in highly sensitive sensing applications [21,22]. Hence there is a demand to have a design based on the TM-pass polarizer in the target wavelength region shorter than 1 μm.

In this paper, a TM-pass/TE-stop integrated polarizer is designed for the 850 nm wavelength region. In order to improve the TM and limit the TE transmission, tilted SWGs are introduced in the proposed polarizer to manipulate the TE effective index solely. After the device geometries optimization, a highest extinction ratio greater than 55 dB and a lowest TM insertion loss less than 0.02 dB is able to be simultaneously achieved in the target wavelength band. Meanwhile, the results show the device working bandwidth, which is defined as the wavelength range that has an extinction ratio higher than 20 dB, and achieves 185 nm under 30 degrees of SWG tilting angle. Furthermore, the insertion loss of the TM polarization state is always less than 0.45 dB in the entire working wavelength band from 756 nm to 941 nm. Moreover, a fabrication tolerance analysis is performed under ±5 nm, ±10 nm, ±15 nm, and ±20 nm SWG ridge width jitters. It shows that the proposed TM-pass polarizer is a relative high fabrication tolerant device which has only 16 nm bandwidth degradation even as the ridge width jitter is 20 nm.

2. Device Structures, Principles, and Optimizations

2.1. Device Structures

Figure 1 shows the 3D schematic diagram of the proposed 850 nm TM-pass/TE-stop polarizer. In order to have a transparent wavelength window shorter than 1 μm, the proposed polarizer is designed on the basis of silicon nitride (Si_3N_4) on an insulator platform with a 500 nm thick wafer and a 2 μm-thick SiO_2 substrate and an air up-cladding. This Differing from the widely used 220 nm-thick wafer, the selected 500 nm-thick waveguide allows the single mode TM polarization state to be confined in the waveguide center as shown in the inset of Figure 1. Otherwise, if a thicker wafer is utilized, it is easy to excite a higher mode TM polarization state. On the contrary, the TM polarization state is probably surrounded at the top and bottom edges of the waveguide, and it will lead to high loss operation. As illustrated in Figure 1, the polarizer's main body is an SWG assisted waveguide which has an overall width of W_1. The core strip width W_2 and the SWG width W_S have to be carefully designed so that the power of the TM polarization state is able to be fully transmitted and the power of the TE polarization state is going to be leaked in the substrate.

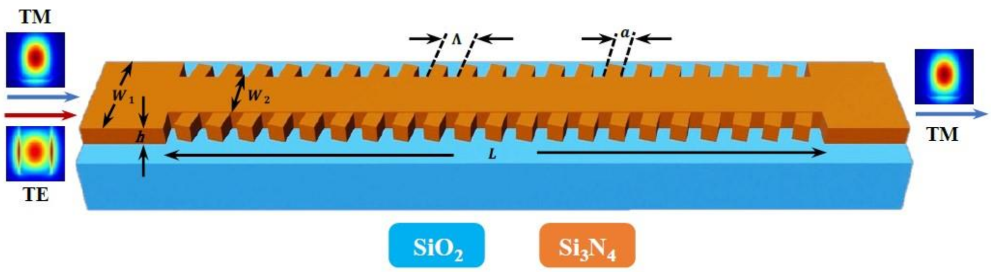

Figure 1. 3D schematic diagram of the proposed 850 nm TM-pass/TE-stop polarizer. W_1: Overall width of the polarizer; W_2: Width of the core strip waveguide; H: Height of the waveguide; L: Length of the polarizer main body; Λ: Period of the SWGs; a: Ridge width of the high indexed material in a single SWG period.

In advance of considering the SWGs, the polarizer is initialized as a pure strip waveguide in a width of W_1 = 200 nm. Under such device geometry conditions, the effective index of the TM polarization state is evaluated to be $n_{eff,TM}$ = 1.504 at 850 nm. Hence the first-order TM mode shown in the inset of Figure 2a is well confined in the center of the strip waveguide. On the other hand, regarding the TE polarization state, its effective index is determined to be $n_{eff,TE}$ = 1.23 at 850 nm. In this case, the TE mode is only surrounded at the edge of the waveguide, as demonstrated in the inset of Figure 2a. Such low TE effective index is much smaller than the material refractive index of the SiO_2 (~1.45 @ 850 nm) and the power of the incident TE polarization state is easy to leak in the substrate.

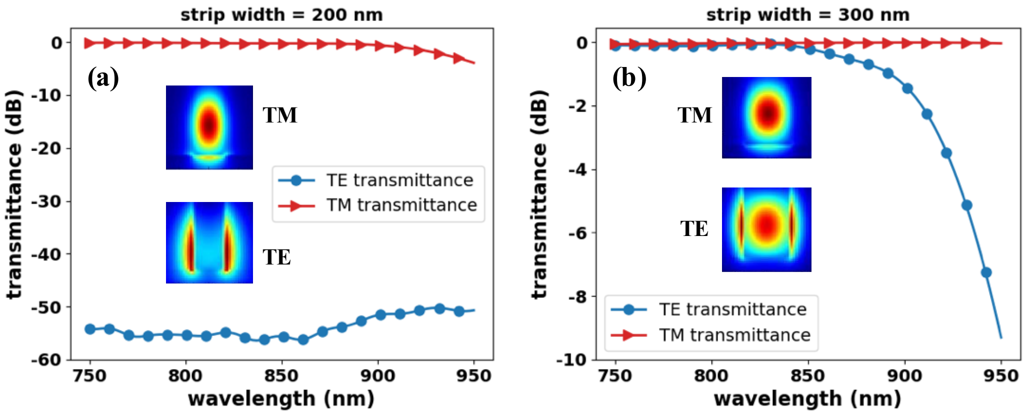

Figure 2. (**a**). Wavelength-dependent transmittances of the TE and TM polarization states under the conditions h = 500 nm and W_1 = 200 nm; (**b**). Wavelength-dependent transmittances of the TE and TM polarization states under the conditions h = 500 nm and W_1 = 300 nm.

By setting the overall length of the polarizer main body to be L = 20 µm, a 3D FDTD simulation is performed to roughly evaluate the wavelength-dependent transmittances for both the TE and TM polarization states, respectively. As demonstrated in Figure 2a, under the above-mentioned device geometries, i.e., W_1 = 200 nm, the transmittances of the TE polarization state are always less than −50 dB over the wavelength range from 750 nm to 950 nm. In other words, only 0.001% of the incident TE power is transmitted. Such low transmittance definitely meets the TE-stop requirements for the proposed polarizer. However, for TM polarization states, though its transmittance looks much higher than the TE polarization state, there is still a notable drop, beginning at around 900 nm, which will reduce both the TM insertion loss and the device extinction ratio, defined in the equations shown below:

$$IL_{TM}(\lambda) = -10log_{10}[P_{in,\,TM}(\lambda)/P_{out,\,TM}(\lambda)] \tag{1}$$

$$ER_{TM}(\lambda) = 10log_{10}[P_{out,\,TM}(\lambda)/P_{out,\,TE}(\lambda)] \tag{2}$$

If the polarizer is desired to work with a higher extinction ratio and then to have a broader working bandwidth, the TM transmittance has to be designed higher in the longer wavelength range, i.e., $\lambda > 900$ nm. To achieve this goal, we simply extend the overall width of the waveguide W_1 from 200 nm to 300 nm and evaluate the wavelength-dependent transmittances again for TE and TM polarization states by performing 3D-FDTD simulations under the same device length, L = 20 µm. As shown in Figure 2b, the TM polarization state is nearly lossless even at a wavelength of 950 nm. Unfortunately, the transmittance of the TE polarization state is also increased dramatically in the entire target wavelength region. According to Equation (2), the extinction ratio, which is defined as the ratio of output TM power over output TE power, will be reduced significantly due to the increased TE transmittance. In order to keep the high TM transmission and restrict the TE transmission simultaneously, the SWGs are introduced in the strip waveguide to replace the extended parts from W_1 = 200 nm to 300 nm.

2.2. SWG Duty Cycle and Period

As specified in [16,23], the SWGs can be treated as a homogenous metamaterial that has engineerable parallel and perpendicular refractive indices estimated as Equations (3) and (4), approximately:

$$n_{\parallel}^2 = \frac{a}{\Lambda}n_H^2 + \left(1 - \frac{a}{\Lambda}\right)n_L^2 \tag{3}$$

$$n_{\perp}^{-2} = \frac{a}{\Lambda} n_H^{-2} + \left(1 - \frac{a}{\Lambda}\right) n_L^{-2} \tag{4}$$

where n_H and n_L are the refractive index of the high and low indexed region, respectively, i.e., Si_3N_4 and SiO_2 in this case; Λ and a stand for the SWG period and ridge width, respectively. With the assumption of an SWG duty cycle of a/Λ = 0.5, on the basis of Equations (3) and (4), the effective indices of TM and TE polarization states are evaluated as 1.64 and 1.37, respectively. In contrast to the pure strip waveguide with W_1 = 300 nm, the TE effective index is now decreased to smaller than the substrate refractive index. Then, the power of the TE polarization state is supposed to be leaked in the substrate. To estimate the transmission performance of such SWG-assisted waveguides, we did the 3D FDTD calculations to work out the wavelength-dependent transmittances under the duty cycle a/Λ = 0.5 and period Λ = 220 nm first. As described by the purple curves in Figure 3a, the transmittance of the TM polarization state is always higher than -0.5 dB over the entire wavelength region from 750 nm to 950 nm. In particular, such a number is always higher than -0.22 dB when the wavelength is shorter than 900 nm. It is equivalent to less than 5% power loss. For the TE polarization state, as depicted with the purple curve in Figure 3b, the transmittance is slightly less than -12 dB at 800 nm, and this number is quickly reduced to smaller than -50 dB at 900 nm. In fact, the TE transmittance at the shorter wavelength region is slightly too large, especially at the region shorter than 800 nm. According to the widely used bandwidth criterion, the extinction ratio has to be higher than 20 dB. However, the -12 dB TE transmittance at this region only gives an extinction ratio less than 12 dB. Hence, the wavelength region shorter than 800 nm is definitely not included in the working wavelength band.

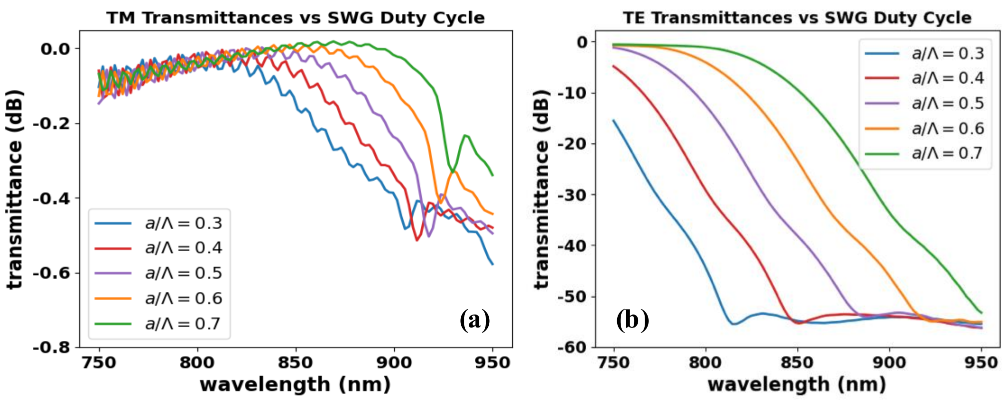

Figure 3. (**a**) The transmittances of TM polarization states as a function of wavelength under the SWG duty cycles from 0.3 to 0.7. (**b**) The transmittances of TE polarization state as a function of wavelength under SWG duty cycles from 0.3 to 0.7.

Since the SWG duty cycle normally has a great impact on the effective indices and then the transmission performances, a number of other SWG duty cycles are attempted to find out a better solution for extinction ratio at shorter wavelength region. After performing the 3D-FDTD simulations under the SWG duty cycle from 0.3 to 0.7, Figure 3a,b show the TM and TE transmittances. With the increasing duty cycle, e.g., $a/\Lambda \geq 0.6$, the TE transmittance is getting higher than -5 dB at 850 nm, which is equivalent to 30% of incident TE power completely transmitted. It is totally unacceptable to meet a high extinction ratio greater than 20 dB. On the other side, when the SWG duty cycle a/Λ is decreased to 0.4, the TE transmittance is reduced to around -29 dB at 800 nm. Meanwhile, the TM transmittance is also higher than -0.5 dB over the entire wavelength region from 750 nm to 800 nm. Both the TE and TM transmittance meet the requirement. If the duty cycle continuously decreased to 0.3, the TE and TM transmittance is also continuously decreased. Generally, the extinction ratio will be increased. However, the TM transmittance at 850 nm to 900 nm looks slightly too small, and such a low SWG duty cycle may challenge the fabrication limits even using electron beam exposure (EBL). Eventually, we selected the SWG duty cycle to be a/Λ = 0.4.

In addition to the duty cycle, the SWG period is another important geometry that has great impact on the polarizer performances. In order to avoid Bragg reflection in the target wavelength band, the SWG period is swept from 160 nm to 240 nm with an increment of 20 nm to evaluate the transmission behavior for both TE and TM polarization states again. As demonstrated in Figure 4a, when the SWG period is 240 nm, the TM transmittance is suddenly dropped to around −30 dB at about 770 nm. Such low transmittance is probably generated due to the Bragg reflections. For the other attempted periods, including Λ = 220 nm, 200 nm, 180 nm, and 160 nm, all the transmittances for the TM polarization states are kept at an acceptable high level over the entire wavelength range. Regarding the TE polarization states, as shown in Figure 4b, all periods have analogues transmission performances. Considering the device fabrication limits, a higher period is preferred. However, as Λ = 220 nm is close to the Bragg window, we selected the period Λ = 200 nm.

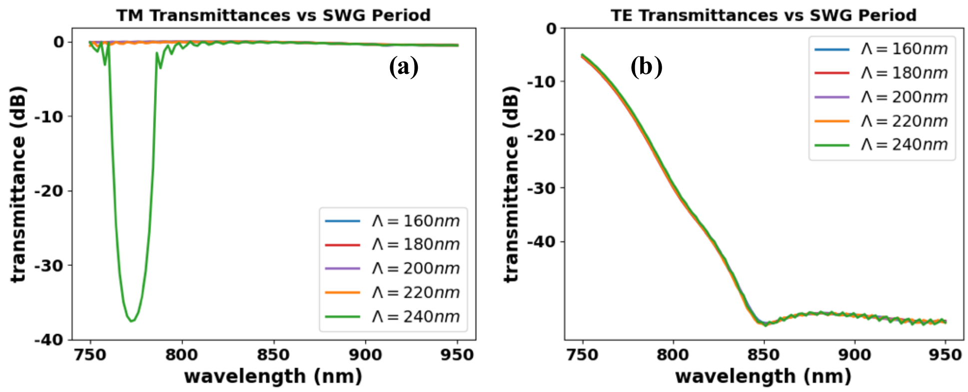

Figure 4. (**a**) The transmittances of the TM polarization state as a function of wavelength under the SWG periods from 160 nm to 240 nm. (**b**) The transmittances of TE polarization state as a function of wavelength under SWG periods from 160 nm to 240 nm.

2.3. SWG Tilting Angle

The SWG ridge tilting angle [24,25] gives additional freedom to improve device performances, especially for polarization management devices. As explained in [24], the tilted SWG has great impact on the TE effective index but has neglected change for the TM polarization state. Owing to this property, we also tilted the SWGs in the proposed polarizer to reduce the TE and maintain the TM effective indices. Firstly, to prove the hypothesis, the effective indices of the TM and TE polarization states are worked out by using band structure analysis [26,27] under different tilting angles. We swept the normalized wavenumber k_n in the propagation direction. When the band diagrams are generated, the peak finding algorithms [20] are utilized to select the resonant wavelength peak for each spectrum. Figure 5a,b are the band diagrams of TM and TE polarization state after wavelength peak finding, respectively. Apparently, the TE polarization state has a notable wavenumber reduction: even the SWGs ridges are only tilted by 10 degrees. But for the TM polarization state, the wavenumber has nearly no changes. Furthermore, we calculated the effective indices as follows [28]:

$$n_{eff}(\lambda_p) = k_n \lambda_p / \Lambda \quad (5)$$

where k_n is the normalized wavenumber at the corresponding resonant wavelength λ_p. As shown in Figure 5c, the TE effective index is reduced by 0.056 at 850 nm when the SWG tilting angle is 30 degrees. For the TM polarization state, as shown in Figure 5d, such effective index reduction at 850 nm is only 0.016. It is clear that the change of TM effective index is less than one third that of the TE effective index. At 900 nm, such effective index reduction is increased to more than 0.073 for TE polarization state. But this number is still around 0.018 for the TM polarization state. From Figure 5a,c, we can find that the first 10 tilting degrees tilting has the most significant effect on the TE effective index reduction, and such an effect is getting weaker and weaker along with the increasing tilting angle. Hence, eventually we select the SWG tilting angle as 30 degrees and no longer increase it.

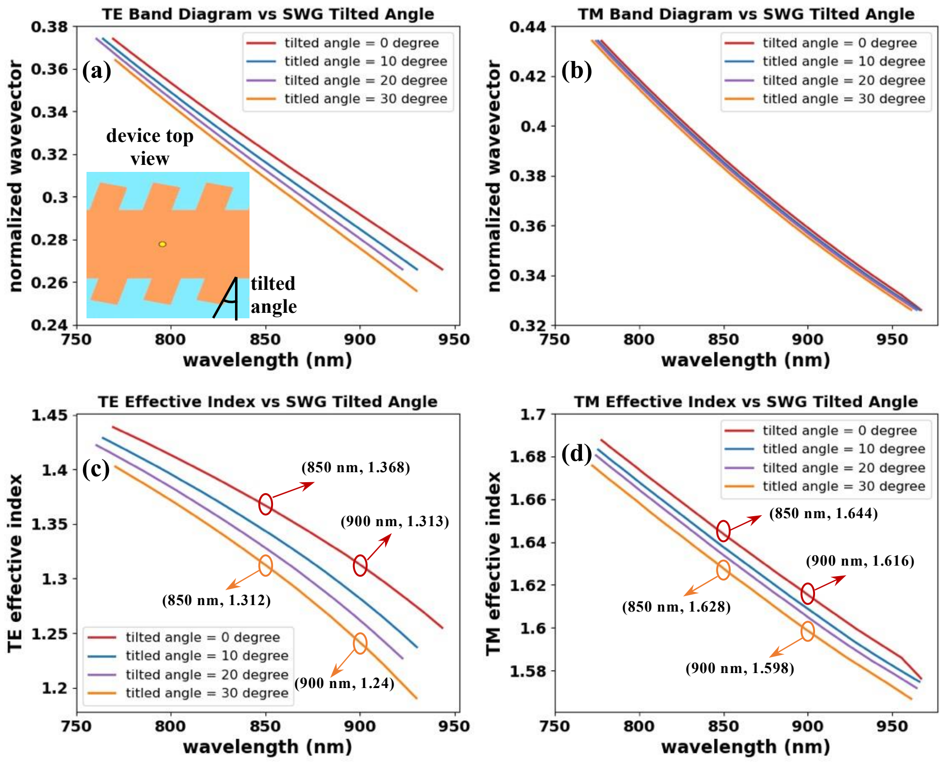

Figure 5. (**a**) Band diagrams of TE polarization states under SWG tilting angle from 0 degree to 30 degrees; (**b**) Band diagrams of TM polarization states under SWG tilting angle from 0 degree to 30 degrees; (**c**) Evaluated TE effective indices under SWG tilting angle from 0 degree to 30 degrees; (**d**) Evaluated TM effective indices under SWG tilting angle from 0 degree to 30 degrees.

3. Results and Discussions

After the device geometries optimization, the full 3D-FDTD simulations were performed to characterize the polarizer performances. Figure 6a is the electric field evolution of the TM polarization state in the XZ plane. Apparently, almost all the incident power is completely transmitted. On the other hand, Figure 6b shows the electric field evolution of the TE polarization state. It is clear that the TE incident power is leaked from the substrate. Visually, it meets the requirement of the TM-pass/TE-stop operation. In spite of this, we also worked out the corresponding extinction ratio and insertion loss in decibels according to the simulated transmittances over the wavelength band from 750 nm to 950 nm. As illustrated in Figure 7, if the polarizer bandwidth is defined as the wavelength region that has extinction ratio greater than 20 dB and insertion loss less than 0.45 dB, the effective operating bandwidth of this proposed polarizer is determined as 185 nm, that is from 756 nm to 941 nm.

Since the device length is one of the most critical parameters for the lightwave transmittances, to have a better transmission performance we tried a number of different lengths L and estimated the corresponding transmittances for TE and TM polarization states, respectively. As shown in Figure 8b, the TE transmittance decreases dramatically with the increasing device length. When the device length is shorter than 20 μm, TE transmittance is too high to have an acceptable extinction in the wavelength region shorter than 800 nm. If only the TE transmittance is considered, L = 30 μm is indubitably the best choice because it has the lowest TE transmittance. However, in Figure 8a, under L $\geq$ 25 μm, there is a non-negligible loss in the wavelength region from 860 nm to 920 nm. Therefore, L = 20 μm is a good trade-off between the device performance in terms of extinction ratio, the insertion loss, and device footprint.

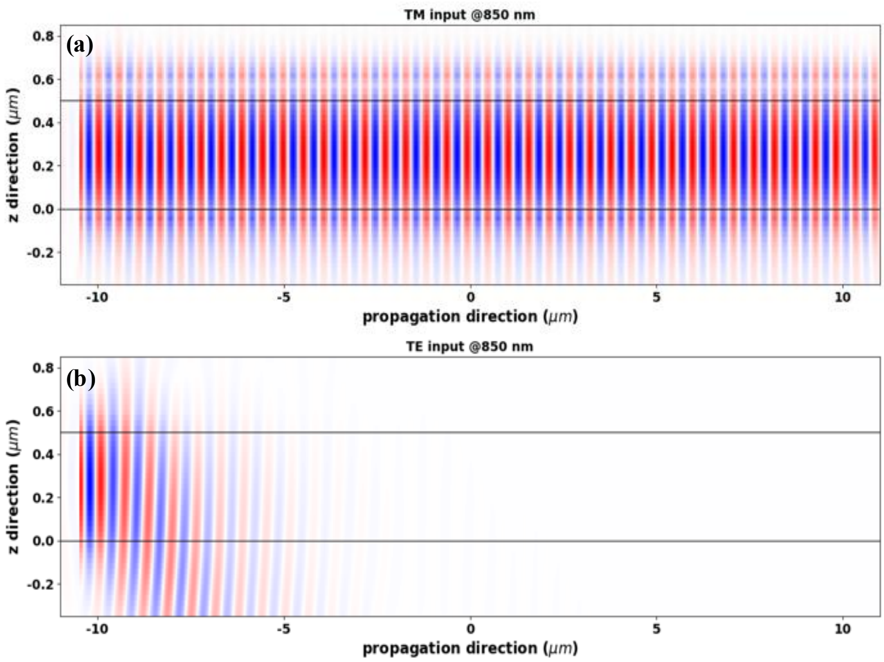

Figure 6. (**a**) Electric field evolution of TM polarization state at 850 nm; (**b**) Electric field evolution of TE polarization state at 850 nm.

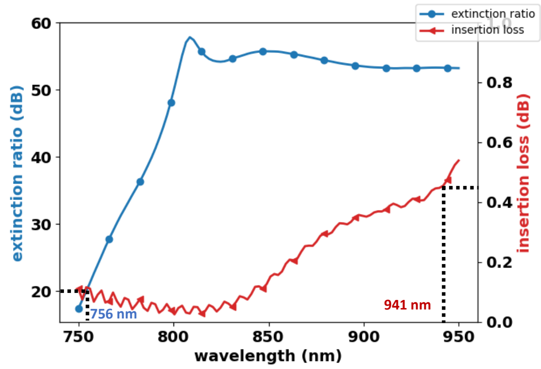

Figure 7. The wavelength dependent extinction ratio (blue circle) and TM insertion loss (red triangle) of the proposed polarizer.

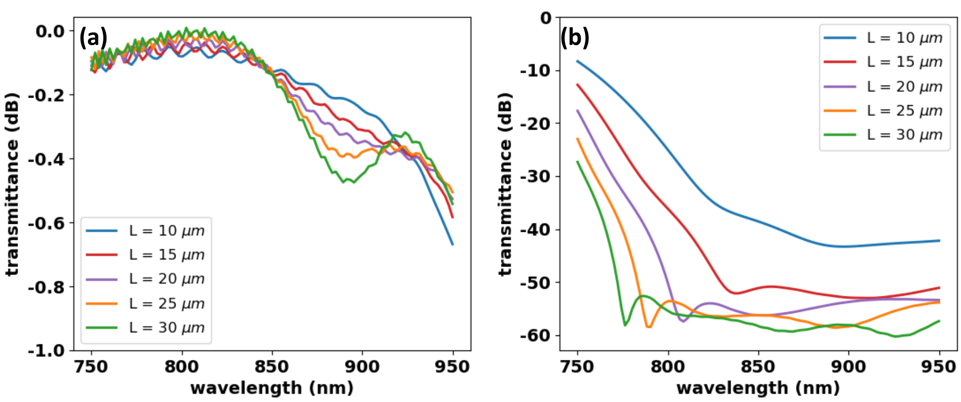

Figure 8. (**a**) Wavelength-dependent transmittances of TM polarization state under various device length from 10 μm to 30 μm; (**b**) Wavelength-dependent transmittances of TE polarization state under various device length from 10 μm to 30 μm.

Fabrication Tolerance Analysis

Considering the fine structure of the tilted SWG, the EBL is suggested to be used to write the device pattern. After developing the photoresistor, the device pattern will be transferred into the silicon nitride wafer by using inductively coupled plasma reactive ion etching. In the above-mentioned fabrication processes, both the EBL writing and etching processes may lead to fabrication errors; we performed fabrication tolerance analysis by introducing SWG ridge width jitters. Figure 9a,b are the evaluated TM and TE transmittance variations under different SWG ridge width jitters from $\pm$ 5 nm to $\pm$ 20 nm. Apparently, from 750 nm to 920 nm, all attempted SWG ridge width jitters result in analogues TM transmission performance. But at the longer wavelength window, i.e., >920 nm, the negative ridge width jitters lead to higher loss for the TM polarization state. As shown in Figure 9b, for the TE polarization state, all the attempted SWG ridge jitters have neglected impact on the transmittance over the wavelength region from 820 nm to 950 nm. But in the shorter wavelength region < 820 nm, the positive jitters, e.g., 5 nm, 10 nm, 15 nm, and 20 nm jitters, increased the TE transmittance by a maximum number of 10 dB. In addition to the transmittances, we also worked out the extinction ratio based on the 3D-FDTD-evaluated TM and TE transmittances by using Equation (2). As demonstrated in Figure 9c, the extinction ratio derived from all the attempted SWG ridge width jitters is always greater than 50 dB in the wavelength region from 800 nm to 950 nm. In the shorter wavelength region, the positive SWG ridge width jitters lead to an extinction ratio reduction by a maximum number of 10 dB. Such a reduction also degrades the device working bandwidth according to the bandwidth definition. Fortunately, even when the ridge jitter is −20 nm, the extinction ratio is greater than 20 dB when the wavelength is longer than 772 nm. Compared with the theoretical result with no jitters, the bandwidth is only reduced by 16 nm. Hence, the proposed polarizer is a relatively high fabrication tolerant device under SWG ridge jitter under $\pm$ 20 nm.

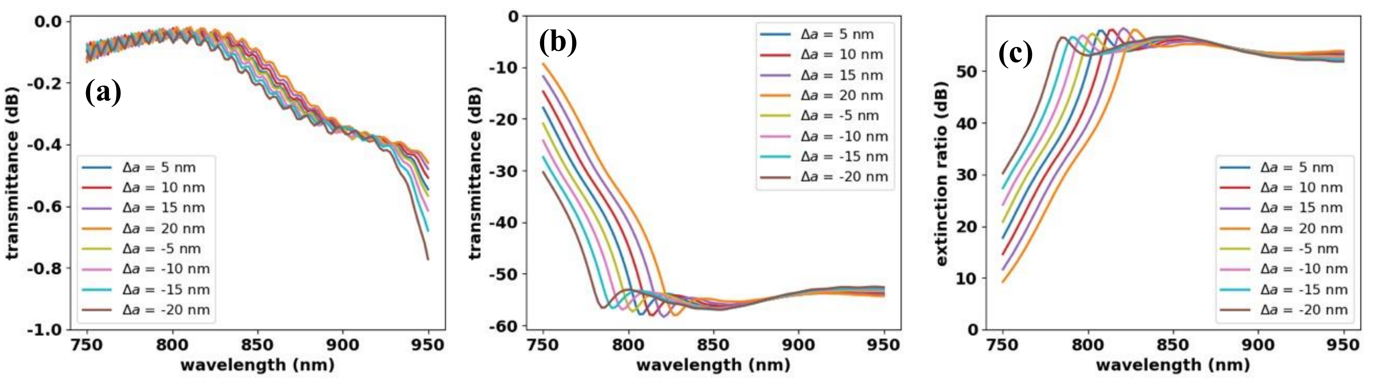

Figure 9. (**a**) Wavelength dependent transmittances of TM polarization state under ±5 nm, ±10 nm, and ±20 nm ridge jitters; (**b**) Wavelength dependent transmittances of TE polarization state under ±5 nm, ±10 nm, and ±20 nm SWG ridge width jitters; (**c**) Extinction ratio evaluated under ±5 nm, ±10 nm, and ±20 nm SWG ridge width jitters.

4. Conclusions

In summary, an 850 nm centered broadband TM-pass/TE-stop polarizer is designed on the Si_3N_4 on insulator platform. With the assistance of tilted SWGs, the proposed polarizer achieves good performances in terms of extinction ratio, operating bandwidth, and insertion loss. Under the device length of 20 μm, the proposed polarizer achieves a high extinction ratio of 55 dB at 850 nm and the working bandwidth, defined as the wavelength region that has extinction ratio higher than 20 dB, is determined to be 185 nm. At the same time, the insertion loss over the entire working wavelength band is always less than 0.45 dB, which is equivalent to higher than 90% of the TM incident power being completely transmitted. Finally, a fabrication tolerance analysis shows that the proposed polarizer is a high fabrication tolerant device in terms of the SWG ridge width. Even the jitter of the SWG ridge width increased to 20 nm, while the working bandwidth is reduced by only 16 nm.

Author Contributions: Conceptualization, Y.D. and Y.X.; Methodology, Y.D.; Software, Y.L.; Validation, Y.L., Y.X. and Y.D.; Formal analysis, Y.L.; Investigation, Y.D. and Y.L.; Resources, Y.D., Y.X. and B.Z.; Data curation, Y.L.; Writing—original draft preparation, Y.D.; Writing—review and editing, Y.D., Y.X. and Y.L.; Visualization, Y.D.; Supervision, Y.D.; Project administration, Y.D.; Funding acquisition, Y.D., Y.X. and B.Z. All authors have read and agreed to the published version of the manuscript.

Funding: This research was funded by the National Natural Science, grant number 6103159, and Natural Science Foundation of Jiangsu Province, grant number BK20190617 and BK20200592.

Data Availability Statement: Not applicable.

Conflicts of Interest: The authors declare no conflict of interest.

References

1. Dai, D.; Bauters, J.; Bowers, J.E. Passive technologies for future large-scale photonic integrated circuits on silicon: Polarization handling, light non-reciprocity and loss reduction. *Light Sci. Appl.* **2012**, *1*, e1. [CrossRef]
2. Sun, H.Y.; Xu, Y.; Dong, Y.; Zhang, B.; Ni, Y. Compact and Broadband on-chip silicon polarization beam splitter based on tilted subwavelength grating. *J. Opt. Soc. Am. B* **2022**, *39*, 3049–3058. [CrossRef]
3. Feng, J.; Akimoto, R.; Zeng, H. Asymmetric Silicon Slot-Waveguide-Assisted Polarizing Beam Splitter. *IEEE Photonics Technol. Lett.* **2016**, *28*, 1294–1297. [CrossRef]
4. Herrero-Bermello, A.; Dias-Ponte, A.; Luque-Gonzales, J.M.; Ortega-Monux, A.; Velasco, A.V.; Cheben, P.; Hair, R. Experimental demonstration of metamaterial anisotropy engineering for broadband on-chip polarization bean splitting. *Opt. Express* **2020**, *28*, 16385–16393. [CrossRef] [PubMed]
5. Chen, J.; Xiao, J. Ultracompact silicon-based polarization splitter and rotator based on asymmetric directional couplers with subwavelength gratings. *J. Opt. Soc. Am. B* **2022**, *30*, 345–354. [CrossRef]
6. Xu, Y.; Xiao, J. Ultracompact and high efficient silicon-based polarization splitter-rotator using a partially-etched subwavelength grating coupler. *Sci. Rep.* **2016**, *6*, 27949. [CrossRef]
7. Luo, Y.; Ge, R.; Luo, H.; Wu, M.; Zhou, L.; Aryal, M.; Li, W.; Yuan, J.; Xu, J.; Lan, Q.; et al. Polarization Splitter-Rotator Based on Multimode Waveguide Gratings. *Crystals* **2021**, *11*, 1170. [CrossRef]
8. Dai, D.; Wang, Z.; Julian, N.; Bowers, J.E. Compact broadband polarizer based on shallowly-etched silicon-on-insulator ridge optical waveguides. *Opt. Express* **2010**, *18*, 27404–27415. [CrossRef] [PubMed]
9. Ni, B.; Xiao, J. Subwavelength grating based compact and broadband TE-pass polarizer for slot waveguides on a SOI platform. *J. Opt. Soc. Am. B* **2019**, *36*, 2126–2133. [CrossRef]
10. Dai, S.; Yu, W.; Zhao, Y.; Li, M.; Li, J.; Zhang, Z.; Liu, J. Broadband and compact TE-pass polarizer based on hybrid plasmonic grating on LNOI platform. *IEEE Photonics J.* **2021**, *13*, 2700109. [CrossRef]
11. Wang, B.; Blaize, S.; Salas-Montiel, R. Nanoscale plasmonic TM-pass polarizer integrated on silicon photonics. *Nanoscale* **2019**, *11*, 20685–20692. [CrossRef] [PubMed]
12. Guan, X.; Chen, P.; Chen, S.; Xu, P.; Shi, Y.; Dai, D. Low-loss ultracompact transverse-magnetic-pass polarizer with a silicon subwavelength grating waveguide. *Opt. Lett.* **2014**, *39*, 4514–4517. [CrossRef] [PubMed]
13. Dong, Y.; Liu, Y.; Xu, Y.; Zhang, B. An Ultra-Broadband Design of TM-pass/TE-Stop Polarizer Based on Multistage Bragg Gratings. *Photonics* **2022**, *9*, 409. [CrossRef]
14. Zhang, Y.; Du, Q.; Wang, C. Monolithic integration of broadband optical isolators for polarization-diverse silicon photonics. *Optica* **2019**, *6*, 315–326. [CrossRef]
15. Firby, C.J.; Chang, P.; Helmy, A.S. Versatile broadband polarization-independent optical circulators for nanophotonic integrated circuits. *J. Opt. Soc. Am. B* **2018**, *35*, 1504–1513. [CrossRef]
16. Cheben, P.; Hair, R.; Schmid, J.H.; Atwater, H.A.; Smith, D.R. Subwavelength integrated photonics. *Nature* **2018**, *560*, 565–572. [CrossRef]
17. Xiong, Y.; Xu, D.; Schmid, J.H.; Cheben, P.; Winne, N.Y. High extinction ratio and broadband silicon TE-pass polarizer using subwavelength grating index engineering. *IEEE Photonics J.* **2015**, *7*, 7802107. [CrossRef]
18. Tinguely, J.C.; Helle, Ø.I.; Ahluwalia, B.S. Silicon nitride waveguide platform for fluorescence microscopy of living cells. *Opt. Express* **2017**, *25*, 27687–27690. [CrossRef]
19. Dong, Y.; Shen, H.; Xu, Y.; Zhang, B. Compact and broadband design of an 850 nm 2x2 3-dB directional coupler with a shallowly etched SWG gap. *App. Opt.* **2022**, *61*, 9154–9162. [CrossRef]
20. Siew, S.Y.; Li, B.; Gao, F.; Zheng, H.Y.; Zhang, W.; Guo, P.; Xie, S.W.; Song, A.; Dong, B.; Luo, L.W.; et al. Review of silicon photonics technology and platform development. *J. Lightwave Technol.* **2021**, *39*, 4373–4389. [CrossRef]
21. Xu, Z.; Lyu, T.; Sun, X. Interleaved Subwavelength Gratings Strip Waveguide Based TM-pass Polarizer on SOI Platform. *IEEE Photonics J.* **2020**, *12*, 4900110. [CrossRef]

22. Densmore, A.; Xu, D.X.; Waldron, P.; Janz, S.; Cheben, P.; Lapointe, J.; Delage, A.; Lamontagne, B.; Schmid, J.H.; Post, E. A Silicon-on-Insulator Photonic Wire Based Evanescent Field Sensor. *IEEE Photonics Technol.* **2006**, *18*, 2520–2522. [CrossRef]
23. Halir, R.; Bock, P.J.; Cheben, P.; Ortega-Moñux, A.; Alonso-Ramos, C.; Schmid, J.H.; Lapointe, J.; Xu, D.; Wangüemert-Pérez, J.G.; Molina-Fernández, I.; et al. Waveguide sub-wavelength structures: A review of principles and applications. *Laser Photonics Rev.* **2015**, *9*, 25–49. [CrossRef]
24. Luque-González, J.M.; Herrero-Bermello, A.; Ortega-Moñux, A.; Sánchez-Rodríguez, M.; Velasco, A.V.; Schmid, J.H.; Cheben, P.; Molina-Fernández, I.; Halir, R. Polarization splitting directional coupler using tilted subwavelength gratings. *Opt. Lett.* **2020**, *45*, 3398–3401. [CrossRef] [PubMed]
25. Yang, J.; Dong, Y.; Xu, Y.; Zhang, B.; Ni, Y. Broadband and high extinction ratio polarization beam splitter on tilted subwavelength gratings. *Appl. Opt.* **2019**, *59*, 7705–7711. [CrossRef] [PubMed]
26. Dong, Y.; Yang, J.; Xu, Y.; Zhang, B.; Ni, Y. On-Chip Beam Splitting Strategies Based on SWG Assisted Directional Coupler. *IEEE Photonics J.* **2021**, *13*, 6600312. [CrossRef]
27. Wang, Y.; Lu, Z.; Ma, M.; Yun, H.; Zhang, F.; Jaeger, N.A.F.; Chrostowski, L. Compact Broadband Directional Coupler Using Subwavelength Gratings. *IEEE Photonics J.* **2016**, *8*, 7101408. [CrossRef]
28. Liu, Y.; Dong, Y.; Xu, Y.; Zhang, B.; Ni, Y. Broadband and high extinction ratio TE-pass/TM-stop polarizer at 850 nm using chirped subwavelength gratings. *Appl. Opt.* **2022**, *61*, 580–587. [CrossRef] [PubMed]